Influence of Surface Snow Properties on an 89-GHz Brightness Temperature Extreme Event at Dome Fuji, Antarctica

Claudio Stefanini, Giovanni Macelloni, *Senior Member, IEEE*, Marion Leduc-Leballeur, and Ghislain Picard

***Abstract*— Microwave brightness temperatures observed in Antarctica at 89 GHz from the advanced microwave sounding unit B (AMSU-B) point out an exceptional decrease of 57 K at Dome Fuji (77.31°S, 39.70°E) during the 2019–2020 summer. The grain size index (GSI) based on 89 and 150 GHz from AMSU-B and independent observations at 89 GHz from the advanced microwave scanning radiometer 2 (AMSR-2) also show concurrent unusual values. To explain such event, a theoretical analysis was carried out by means of a radiative transfer model. We explore the sensitivity of brightness temperature to surface snow properties focusing on December, just before the decrease, and April, at its end. Results confirm that this variation is mainly related to an increase in snow grain size. A decrease in snow density is also involved as suggested by the increase in brightness temperature at 1.4 GHz from soil moisture and ocean salinity (SMOS) and in the polarization ratio at 36 GHz from AMSR-2. Extreme values observed at multiple frequencies, as well as peculiar atmospheric conditions explored in a previous study, confirm the uniqueness of this event at least on decennial scale.**

***Index Terms*— Advanced microwave sounding unit B (AMSU-B), cryosphere, microwave radiometry, modeling.**

I. Introduction

PASSIVE microwave observations over Antarctica have been collected for more than 40 years at different frequencies. They allow monitoring the ice sheets at different depths, from a few centimeters at >100 GHz to several hundred meters at 1.4 GHz [1], [2]. First, studies used 19 and 37 GHz to investigate surface or near-surface properties such as air temperature changes [1], snow layering [3], snow grain size [4], and snow density [5]. Snow accumulation has been estimated from 7 GHz [6]. More recently, it was demonstrated that also at 1.4 GHz, information about snow surface properties and the process of metamorphism can be derived [7], [8].

Manuscript received 8 September 2023; revised 24 January 2024; accepted 12 February 2024. Date of publication 19 February 2024; date of current version 28 February 2024. *(Corresponding author: Claudio Stefanini.)*

Claudio Stefanini is with the Institute of Applied Physics Nello Carrara, National Research Council, 50019 Sesto Fiorentino, Italy, and also with the Dipartimento di Scienze Ambientali, Informatica e Statistica, DAIS, Ca' Foscari University of Venice, Venice, 30170 Mestre, Italy (e-mail: claudio.stefanini@unive.it).

Giovanni Macelloni and Marion Leduc-Leballeur are with the Institute of Applied Physics Nello Carrara, National Research Council, 50019 Sesto Fiorentino, Italy.

Ghislain Picard is with Université Grenoble Alpes, CNRS, Institut des Géosciences de l'Environnement (IGE), UMR 5001, 38400 Grenoble, France.

Digital Object Identifier 10.1109/LGRS.2024.3367111

A grain size index (GSI) has been developed from 89 and 150 GHz brightness temperatures (T_B) by [9] as a proxy of the snow grain radius in the topmost centimeters of the snowpack. The study of some summer extreme increases in GSI observed on the East Antarctica highlighted that these variations are deeply connected with the meteorological conditions at seasonal and interannual time scales [10]. Meteorological features such as low wind speed and low skin temperature during the summer were identified as the main drivers leading to these unusual grain size conditions. The most intense seasonal event has been identified at Dome Fuji during the 2019–2020 austral summer, when the snow grains reached the largest size as well as the fastest growing rate [10].

These observations could help to detect sharp changes in surface properties and monitor the effect of anomalous atmospheric conditions. Besides, coarse-grained snow has a lower albedo than thinner, therefore changes in snow grain size can impact the overall energy balance of the region and influence local and regional climate conditions [9].

In this letter, the Dome Fuji event was analyzed by means of snow emission modeling in order to better understand the quantitative relationship between T_B and surface properties at 89 GHz during the austral summer, beyond the GSI proxy. Section II presents the satellite and meteorological datasets. Section III describes the electromagnetic model for the T_B simulations, the thermal model to estimate the snowpack temperature, and the atmospheric model to describe the attenuation of the microwave signals. Section IV presents simulation results and discusses them with information coming from other frequencies. Section V draws conclusions.

II. Data

A. Advanced Microwave Sounding Unit B

From the advanced microwave sounding unit B (AMSU-B), we selected T_B at 89 and 150 GHz in the range of incidence 0–25° (downloaded from https://www.avl.class.noaa.gov/). The GSI, defined as $\text{GSI} = 1 - T_B(150\ \text{GHz})/T_B(89\ \text{GHz})$ [9], is computed for Dome Fuji from July 2012 to June 2023. It is a proxy of the near-surface snow grain radius, therefore, it provides approximate information only, and may also be influenced by other snow and atmospheric properties.

B. Advanced Microwave Scanning Radiometer 2

The advanced microwave scanning radiometer 2 (AMSR-2) on-board Japan's Global Change Observation Mission

1st - Water "SHIZUKU" (GCOM-W1) satellite provides T_B at 89, 36, and 18 GHz at horizontal and vertical polarizations and for incidence angle of 55°. Daily mean T_B are extracted over Antarctica from the Level 3 product provided by the JAXA's Globe Portal System (G-Portal, https://gportal.jaxa.jp/) in the Southern polar stereographic projection with a resolution of 25 km. Data from July 2012 to June 2023 are considered here.

C. SMOS

The soil moisture and ocean salinity (SMOS) satellite from the European Space Agency (ESA) provides a multiangular T_B at 1.4 GHz. From the SMOS Level 3 product delivered by the Center Aval de Traitement des Données SMOS (https://www.catds.fr/, [11]), we extracted daily T_B from July 2012 to June 2023 over the 50°–55° range of incidence angles. The product is georeferenced on the Equal-Area Scalable Earth version 2.0 (EASE–Grid2) grid in the Southern Hemisphere Azimuthal projection with a 25 km resolution.

D. Ocean and Land Color Instrument

The ocean and land color instrument (OLCI) instrument on board the ESA's Copernicus Sentinel-3A/B is used to estimate the specific surface area (SSA) of snow at 1 cm below the surface [12]. The grain radius r is then computed as $r = 3/(\rho_{\text{ice}} \cdot \text{SSA})$ where $\rho_{\text{ice}} = 917\ \text{kg m}^{-3}$ is the ice density.

E. ERA5

Meteorological parameters on single and pressure levels are taken from the ERA5 reanalysis produced by the European Center for Medium-Range Weather Forecasts [13, ECMWF]. Data are provided over a regular latitude–longitude grid of 0.25° resolution, and we reprojected them to the Southern polar stereographic projection. We considered daily mean over 2012–2023 and also hourly values as input for the snowpack temperature estimation.

III. Methods

A. Snow Microwave Radiative Transfer Model

T_B simulations at 89 and 150 GHz were conducted with the Snow Microwave Radiative Transfer model (SMRT; [14]). Among the available electromagnetic scattering theories in SMRT, we selected the symmetrized strong contrast expansion method to ensure a continuous scattering function over the whole range of ice fractions (i.e., snow density) allowing a good description at intermediate densities (∼500 kg m^{-3}) and high frequencies [15]. In the model, the snowpack is represented as a multilayered medium, each layer being defined by the thickness, density, temperature, and microwave grain size [16]. We used the scaled exponential microstructure model, recommended to simulate high microwave frequencies [17], [18], and a newly defined microwave grain size which is the product of the Porod length and a polydispersity $K = 0.63$ optimized for the Antarctic Plateau [16].

The simulations are performed at 0°–25° of incidence angle matching to the AMSU-B observations. At 89 and 150 GHz, the microwave emanation depth (also known as penetration depth or e-folding depth) is estimated a few centimeters [1], [9], therefore, we defined the snowpack as a stack of 5 cm layers from the surface to 2 m in depth, then an infinite ice layer for completion. Over the 2 m snowpack, the density is kept constant (350 kg m^{-3} [19], [20]), and the snow grain radius profile decreases linearly from 0.10 mm at the surface [20] to 0.15 mm at 50 cm and from 0.15 mm at 50 cm to 0.30 mm at 1 m [5]. Below 2 m, the infinite layer has a density at 350 kg m^{-3}, and radius at 0.30 mm.

TABLE I

$T_B^{\uparrow}$, $T_B^{\downarrow}$, t in December and April for 89 and 150 GHz Over Dome Fuji According to the Rosenkranz's (1998) Model

	89 GHz		150 GHz	
	December	April	December	April
$T_B^{\uparrow}$	7.3 K	5.9 K	7.8 K	3.5 K
$T_B^{\downarrow}$	10.5 K	9.1 K	12.0 K	7.6 K
t	0.969	0.974	0.967	0.985

B. Snowpack Temperature

The temperature profile required by SMRT is estimated with the surface energy budget and thermal diffusion model called Minimal Firn Model [9], [21], [22] (MFM, https://github.com/ghislainp/mfm). We used as inputs skin temperature, 2 m temperature, 10 m wind speed, snowfall, surface pressure, cloud cover, and surface downward long–wave and short–wave radiation flux from the hourly ERA5 reanalysis. The output are averaged to obtain the daily snowpack temperature profiles in December and April. The 10 m temperature in depth is fixed at 222.7 K, equal to the annual mean temperature at Dome Fuji [13], [23].

C. Atmospheric Microwave Emission and Transmission

The atmosphere influences the microwave emission from the Earth surface: 1) emission coming from the surface is attenuated by the atmosphere and 2) the atmosphere emits radiation due to its own temperature in both upward and downward direction [24]. The last contribution, once reflected by the surface, is then redirected toward to the sensor and contributes to the measured T_B. In general, the atmospheric contribution at these frequencies is low over the Antarctica Plateau because of the low atmospheric humidity and high elevation (low atmospheric mass/high geopotential) [21]. The upward $T_B^{\uparrow}$ and downward $T_B^{\downarrow}$ atmospheric brightness temperature and transmittance t are computed with a simple nonscattering microwave radiative transfer model [25]. The model inputs are air temperature, geopotential height, water vapor density, and ozone molecules density over the 24 pressure levels provided by ERA5 from the ice surface up to 40 km above the considered point.

The calculated $T_B^{\uparrow}$, $T_B^{\downarrow}$, transmittance t are calculated in December and April for 89 and 150 GHz from 0° to 25° of incidence angle. Their variability within this incidence range is low in these atmospheric conditions (standard deviation of 0.1 and 0.3 K for T_B and ∼0.001 for t), and we used the mean values during T_B simulations to save computational resources (Table I).

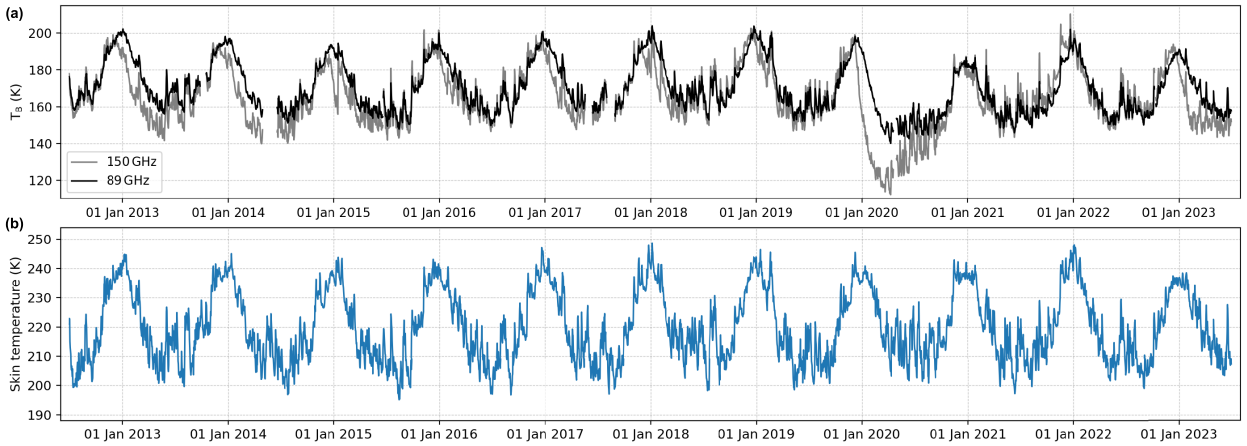

Fig. 1. (a) T_B from July 2012 to June 2023 at Dome Fuji at (Black) 89 GHz and (Gray) 150 GHz from AMSU-B and (b) skin temperature from ERA5.

IV. Analysis

A. Brightness Temperature Observations

Fig. 1(a) shows 89 GHz T_B from AMSU-B from July 2012 to June 2023 at Dome Fuji. The 11-year T_B time series shows an annual variation between December and April of 46.1 ± 1.9 K over July 2012–June 2023, which at first order follows the air temperature seasonal variations [Fig. 1(b), 48.3 ± 3.2 K on average]. A faster and higher seasonal decrease happened from December 2019 and reached a minimum on 10 April 2020. T_B decreased by 57 K in four months reaching 140.1 K. This minimum was never observed during the 11-year studied period, and is about 15 K lower than the usual minimum of this month. After this, T_B slowly increased, but remained lower than usual during the whole winter. From AMSU-B, we also observed a decrease of 82 K at 150 GHz, while the climatological value is 57.3 ± 3.4 K [Fig. 1(a)].

Note that AMSR-2 observations (not shown) also recorded an exceptional decrease of 65–70 K at 89 GHz, above the climatological mean of 50.7 ± 5.9 K and 52.1 ± 7.0 K for horizontal and vertical polarization, respectively. The difference with AMSU-B derives from the different incidence angle.

In the T_B decreasing period, the skin temperature decreased by 45 K, which is within the average seasonal variations. This suggests that the 89 GHz observations are affected by others factors than temperature as ∼75% of the total T_B variations observed at 89 GHz and ∼50% of the total variations at 150 GHz can be explained by the seasonal temperature variations. The sensitivity to snow grain size and density in surface is analyzed in the following.

B. Sensitivity Tests

In order to explore the complete range of variability of the T_B at 89 GHz, two specific dates were considered for the simulations. The first case study is on 10 December 2019 when the T_B at 89 GHz reached its annual maximum. The surface temperature of the snowpack was 245 K according to the ERA5 skin temperature. The second case study is on 10 April 2020 when the T_B at 89 GHz reached its annual minimum with a ERA5 skin temperature of 205 K. Since the GSI is a combination of the 89 and 150 GHz, we also simulated the behavior of the 150 GHz T_B.

TABLE II

Emanation Depths at 89 and 150 GHz, Observed T_B Decrease From December 2019 to April 2020 and Modeled Changes in the Snow Grain Radius Considering Three Different Surface Densities

		89 GHz	150 GHz
	Emanation depth	∼20 cm	∼4 cm
	T_B decrease	57 K	82 K
Radius change	at 200 kg m^{-3}	0.23 mm	0.14 mm
	at 300 kg m^{-3}	0.23 mm	0.15 mm
	at 400 kg m^{-3}	0.25 mm	0.24 mm

To evaluate the T_B sensitivity to the surface snow properties, we varied the snow grain radius in the first layer (5 cm thick) from 0.05 to 0.50 mm, and for three values of surface layer density (200, 300, and 400 kg m^{-3}). Fig. 2(a) and (b) show the simulated T_B at 89 GHz for 10 December 2019 and 10 April 2020, respectively, for the three values of surface density. Fig. 2(c) and (d) shows the same at 150 GHz. The shadows in figures refer to a variation of the skin temperature of ±2 K and the consequent modified snowpack temperature profiles estimated by the MFM, in order to appreciate a possible uncertainty of the ERA5 estimation [26]. Simulation results show low sensitivity to this uncertainty.

The simulations at 89 GHz show that the observed decrease of 57 K from December to April corresponds to an increase of the radius of 0.23 and 0.25 mm at 200 and 400 kg m^{-3}, respectively. At 150 GHz, the observed T_B decrease of 82 K corresponds to an increase of 0.14 and 0.24 mm, respectively (Fig. 2, Table II). The difference is linked to a distinct sensibility of the two frequencies, being the emanation depth ∼20 cm at 89 GHz and ∼4 cm at 150 GHz [9]. Thus, the snow temperature closer to the surface experience larger oscillations and generate a larger T_B annual variability at 150 GHz than 89 GHz. The simulations show that the measured minimum T_B [Fig. 2(b) and (d)] can be only explained by a large value of the snow grain radius. The surface density variation also affect T_B at both frequencies, but an increase in grain size is always needed to explain the whole observed decrease in T_B.

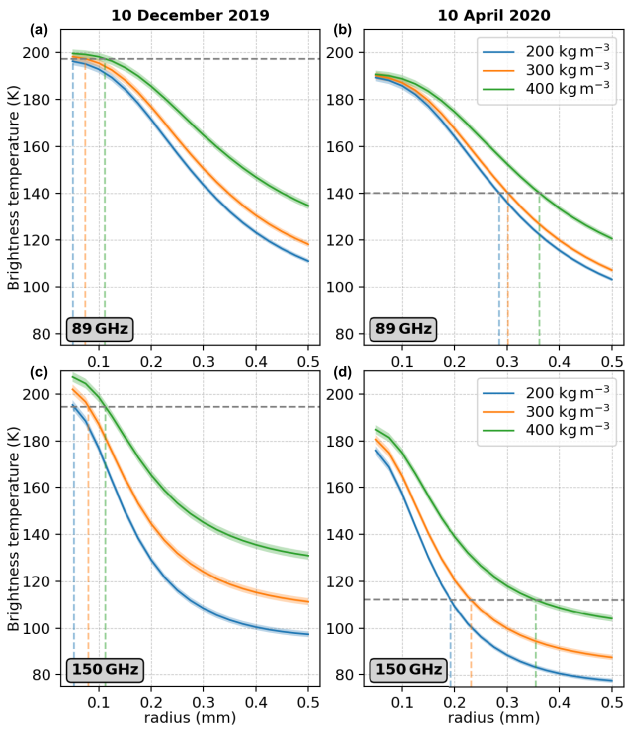

Fig. 2. Simulated brightness temperature at 89 and 150 GHz as a function of the snow grain radius for three surface snow densities (color lines) for the conditions when the observed T_B (dotted gray lines) was (a) and (c) maximum (10 December 2019) and (b) and (d) minimum (10 April 2020). The shadows cover simulations with variations of ±2 K in the skin temperature.

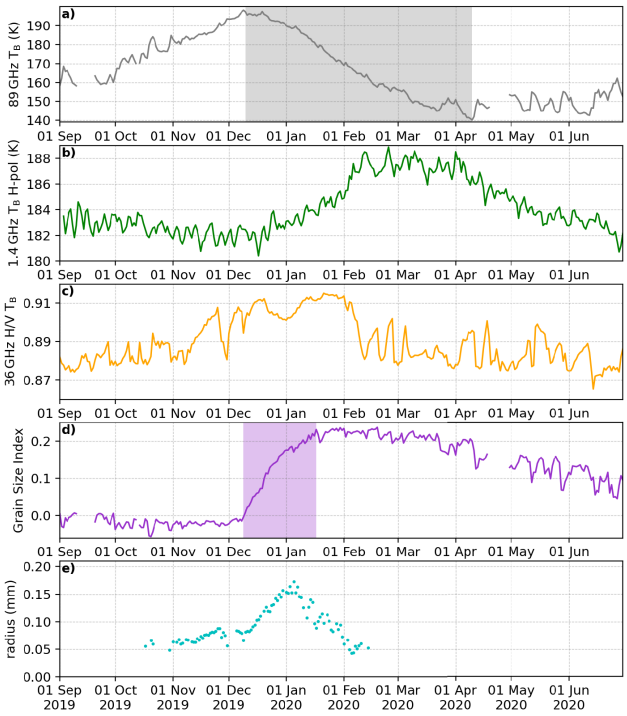

Fig. 3. (a) Brightness temperature from 1 September 2019 to 30 June 2020 at Dome Fuji at 89 GHz from AMSU-B, the gray area covers the period from the T_B maximum (10 December) to the minimum (10 April). (b) Brightness temperature at 1.4 GHz in horizontal polarization from SMOS. (c) Polarization ratio at 36 GHz from AMSR-2. (d) GSI from AMSU-B, the purple area covers the grain size seasonal increase as defined in [10]. (e) Snow grain radius from OLCI.

C. Indications From Independent Measurements

The sensitivity analysis show that both snow grain size and surface density influence the 89 GHz T_B. To untangle their respective influence, we considered also independent datasets to better describe the snow surface changes.

At 1.4 GHz, T_B in horizontal polarization is usually stable with on average 184.1 ± 2.1 K over July 2012–June 2023. However, between December 2019 and February 2020, T_B increased by about 7 K with a maximum of 188.9 K [Fig. 3(b)] never observed by SMOS at Dome Fuji over 2012–2023 whereas T_B in vertical polarization remained stable. As snow grains have no influence at 1.4 GHz [27], this is an indicator of a decrease in surface density. Indeed, a previous work highlighted a variation of the 1.4 GHz T_B in horizontal polarization with the same order of magnitude at Dome C in 2014–2015 [7]. It showed that the increase in T_B was related to a decrease in surface density and an increase of the thickness of the uppermost layer, linked to the formation of surface hoar and/or snow accumulation facilitated by a period of a few months with lower than normal speed of wind. In situ measurements at Dome C showed that the surface snow density reached values below 300 kg m^{-3}.

A decrease (increase) in the polarization ratio (H/V) at 36 GHz is linked to an increase (decrease) in the snow density in the topmost 3 cm layer [5]. On average, it has an annual variation of 0.046 ± 0.001 over July 2012–June 2023, with a mean maximum of 0.907 ± 0.002 [Fig. 3(c)]. During the 2019–2020 event, the maximum was 0.915, the highest of the entire time series, and values were maintained high during all January with a mean of 0.911 (+0.025 with respect to 2013–2023 January climatology). This confirms the possibilities of a near-surface density below 300 kg m^{-3}, as in [5]. The polarization ratio reached its maximum in the second half of January, meaning that the snow density of the 0–3 cm layer had a minimum during this period. The different behavior of 1.4 and 36 GHz [Fig. 3(b) and (c)] can be not only due to a different emanation length of these frequencies but also to the sensitivity of 1.4 GHz to variations in the surface elevation [7]. Snowfall occurred starting from the mid-January [10], leading to a possible increase of the first snowpack layer and hence an increase of the 1.4 GHz T_B. By modeling, we examined the effect of an increase of the topmost layer thickness in April, up to +3 cm (i.e., 8 cm in total for the first layer). Simulation showed that for a radius of 0.30 mm and fixed density, the increase of thickness causes a decrease of ∼10–15 K (higher for lower density) at 89 GHz and only ∼2–5 K at 150 GHz.

The snow surface roughness also affects the T_B observations, and it could be monitoring with the polarization ratio [5]. The roughness is mainly frequency-dependent. However, in our case, the polarization ratios at 18, 36, and 89 GHz observed from AMSR-2 (not shown) exhibit similar trend and high values (0.854 ± 0.003, 0.911 ± 0.004, 0.945 ± 0.003, respectively, in January 2020). This suggests that the surface roughness has a weak effect and the polarization ratio is mainly related to the surface density variations.

In parallel, the GSI increased from December to mid-January [Fig. 3(d)] whereas skin temperature was relatively stable (237.9 ± 2.3 K). The radius estimates from the OLCI SSA [Fig. 3(e)] also pointed out an increase of grain size in the first centimeter of snow with a maximum at the beginning of

TABLE III
MAXIMUM VARIATIONS OF THE PARAMETERS OF FIG. 3(b)–(e)

T_B H-pol 1.4 GHz	H/V T_B 36 GHz	GSI	Radius
+8.5 K	+0.034	+0.266	+0.13 mm

January. Then, the values decreased but the stable GSI suggest that grain size remained high during a more long time below the surface. Therefore, the decrease in T_B at 89 GHz can be mainly explained by an increase in the grain size, from mid-December to mid-0January, and, with a lower magnitude, by a decrease in snow density. Table III summarizes the maximum variations during the 2019–2020 summer.

V. CONCLUSION

We analyzed the stronger than usual decrease in brightness temperature (T_B) at 89 GHz during the 2019–2020 summer at Dome Fuji observed by the AMSU-B and AMSR-2 microwave radiometers. Theoretical analysis has been performed by using the SMRT to assess the sensitivity of this event to changes in snow surface properties. The simulations confirm the sensitivity of 89 GHz T_B to snow grain size and density in the first centimeters.

Additional surface density and snow grain size information during the event have been obtained from T_B at 1.4 GHz from SMOS, polarization ratio at 36 GHz from AMSR-2, the GSI computed from AMSU-B observations, and the OLCI snow grain radius. Comparisons show a rapid increase in surface grain size from December to January, installing large snow grains until April, concomitant to snow density lower than usual from January. This corresponds to the signature of surface hoar [7]. We conclude that the unusual observed 89 GHz T_B variation can be explained by the presence of unusual large snow grain size and low surface density.

This analysis highlights the importance of high frequencies for monitoring of the Antarctic ice sheet and to detect anomalous surface changes, which can impact the surface energy balance.

REFERENCES

[1] S. Surdyk, "Using microwave brightness temperature to detect short-term surface air temperature changes in Antarctica: An analytical approach," *Remote Sens. Environ.*, vol. 80, no. 2, pp. 256–271, May 2002.

[2] G. Macelloni, M. Leduc-Leballeur, M. Brogioni, C. Ritz, and G. Picard, "Analyzing and modeling the SMOS spatial variations in the east Antarctic Plateau," *Remote Sens. Environ.*, vol. 180, pp. 193–204, Jul. 2016.

[3] G. Macelloni, M. Brogioni, P. Pampaloni, and A. Cagnati, "Multifrequency microwave emission fromthe Dome-C area on the east Antarctic Plateau: Temporal and spatial variability," *IEEE Trans. Geosci. Remote Sens.*, vol. 45, no. 7, pp. 2029–2039, Jul. 2007.

[4] L. Brucker, G. Picard, and M. Fily, "Snow grain-size profiles deduced from microwave snow emissivities in Antarctica," *J. Glaciology*, vol. 56, no. 197, pp. 514–526, 2010.

[5] N. Champollion et al., "Marked decrease in the near-surface snow density retrieved by AMSR-E satellite at dome C, Antarctica, between 2002 and 2011," *Cryosphere*, vol. 13, no. 4, pp. 1215–1232, Apr. 2019.

[6] R. J. Arthern, D. P. Winebrenner, and D. G. Vaughan, "Antarctic snow accumulation mapped using polarization of 4.3-cm wavelength microwave emission," *J. Geophys. Res. Atmos.*, vol. 111, no. D6, pp. 1–10, Mar. 2006.

[7] M. Leduc-Leballeur et al., "Influence of snow surface properties on L-band brightness temperature at dome C, Antarctica," *Remote Sens. Environ.*, vol. 199, pp. 427–436, Sep. 2017.

[8] L. Brucker, E. P. Dinnat, G. Picard, and N. Champollion, "Effect of snow surface metamorphism on aquarius L-band radiometer observations at dome C, Antarctica," *IEEE Trans. Geosci. Remote Sens.*, vol. 52, no. 11, pp. 7408–7417, Nov. 2014.

[9] G. Picard, F. Domine, G. Krinner, L. Arnaud, and E. Lefebvre, "Inhibition of the positive snow-albedo feedback by precipitation in interior Antarctica," *Nature Climate Change*, vol. 2, no. 11, pp. 795–798, Jul. 2012.

[10] C. Stefanini, G. Macelloni, M. Leduc-Leballeur, V. Favier, B. Pohl, and G. Picard, "Extremes of surface snow grains change in east Antarctica and their relationship with meteorological conditions," *The Cryosphere*, vol. 18, no. 2, pp. 593–608, Feb 2024.

[11] A. Al Bitar et al., "The global smos level 3 daily soil moisture and brightness temperature maps," *Earth Syst. Sci. Data*, vol. 9, no. 1, pp. 293–315, Jun. 2017.

[12] S. Arioli, G. Picard, L. Arnaud, and V. Favier, "Dynamics of the snow grain size in a windy coastal area of Antarctica from continuous in situ spectral-albedo measurements," *Cryosphere*, vol. 17, no. 6, pp. 2323–2342, Jun. 2023.

[13] H. Hersbach et al., "The ERA5 global reanalysis," *Quart. J. Roy. Meteorol. Soc.*, vol. 146, no. 730, pp. 1999–2049, Jun. 2020.

[14] G. Picard, M. Sandells, and H. Löwe, "SMRT: An active–passive microwave radiative transfer model for snow with multiple microstructure and scattering formulations (V1.0)," *Geosci. Model Develop.*, vol. 11, no. 7, pp. 2763–2788, Jul. 2018.

[15] G. Picard, H. Löwe, and C. Mätzler, "Brief communication: A continuous formulation of microwave scattering from fresh snow to bubbly ice from first principles," *Cryosphere*, vol. 16, no. 9, pp. 3861–3866, Sep. 2022.

[16] G. Picard et al., "The microwave snow grain size: A new concept to predict satellite observations over snow-covered regions," *AGU Adv.*, vol. 3, no. 4, pp. 1–9, Jul. 2022.

[17] M. Sandells et al., "Simulation of Arctic snow microwave emission in surface-sensitive atmosphere channels," *EGUsphere*, to be published. Accessed: Aug. 2023. [Online]. Available: https://egusphere.copernicus.org/preprints/2023/egusphere-2023-696/

[18] C. Vargel et al., "Arctic and subarctic snow microstructure analysis for microwave brightness temperature simulations," *Remote Sens. Environ.*, vol. 242, Jun. 2020, Art. no. 111754.

[19] Hondoh et al., "Basic analyses of dome Fuji deep ice core Part 2: Physical properties," *Polar Meteorol. Glaciol.*, vol. 13, pp. 90–98, Dec. 1999.

[20] Q. Libois, G. Picard, L. Arnaud, S. Morin, and E. Brun, "Modeling the impact of snow drift on the decameter-scale variability of snow properties on the Antarctic Plateau," *J. Geophys. Res. Atmos.*, vol. 119, no. 20, pp. 11662–11681, Oct. 2014.

[21] G. Picard, L. Brucker, M. Fily, H. Gallée, and G. Krinner, "Modeling time series of microwave brightness temperature in Antarctica," *J. Glaciol.*, vol. 55, no. 191, pp. 537–551, 2009.

[22] F. Domine, G. Picard, S. Morin, M. Barrere, J. Madore, and A. Langlois, "Major issues in simulating some Arctic snowpack properties using current detailed snow physics models: Consequences for the thermal regime and water budget of permafrost," *J. Adv. Model. Earth Syst.*, vol. 11, no. 1, pp. 34–44, Jan. 2019.

[23] Y. Wang and S. Hou, "Spatial distribution of 10 m firn temperature in the Antarctic ice sheet," *Sci. China Earth Sci.*, vol. 54, no. 5, pp. 655–666, Oct. 2010.

[24] P. W. Rosenkranz, "Rough-sea microwave emissivities measured with the SSM/I," *IEEE Trans. Geosci. Remote Sens.*, vol. 30, no. 5, pp. 1081–1085, Sep. 1992.

[25] P. W. Rosenkranz. *Line-By-Line Microwave Radiative Transfer (Non-Scattering)*. Accessed: Aug. 2023. [Online]. Available: http://cetemps.aquila.infn.it/mwrnet/lblmrt_ns.html

[26] J. Zhu, A. Xie, X. Qin, Y. Wang, B. Xu, and Y. Wang, "An assessment of ERA5 reanalysis for Antarctic near-surface air temperature," *Atmosphere*, vol. 12, no. 2, p. 217, Feb. 2021.

[27] C. Mätzler, "Applications of the interaction of microwaves with the natural snow cover," *Remote Sens. Rev.*, vol. 2, no. 2, pp. 259–387, Jan. 1987.

Open Access funding provided by 'Università Ca' Foscari Venezia' within the CRUI CARE Agreement